UNIVERSITY OF CALIFORNIA SAN DIEGO

# Time- and Circadian-Dependent Fluctuations of Mammalian Nuclear Reorganization

A Thesis submitted in partial satisfaction of the requirements

for the degree Master of Science

in

Biology

by

Nicolette Marie Allaway

Committee in charge:

Professor Mark Ellisman, Chair
Professor Brenda Bloodgood, Co-chair
Professor Gulcin Pekkurnaz

2019

The Thesis of Nicolette Marie Allaway is approved, and it is acceptable in quality and form for publication on microfilm and electronically:

_____

_____

Co-chair

_____

Chair

University of California San Diego

2019

DEDICATION

I’d like to dedicate this thesis to my parents, JoAnne and John.

Thank you for making everything in my life possible. Your unconditional love and commitment to my success mean the world to me.

TABLE OF CONTENTS

LIST OF FIGURES

# ACKNOWLEDGEMENTS

I would like to thank Dr. Matthias Haberl for his unwavering support and patience as my advisor. Because of him I have learned invaluable skills as a scientist and a person.

I would also like to thank my committee chair Dr. Mark Ellisman and the members of NCMIR for their help on this project. I would especially like to thank Andrea Thor and Mason Mackey for their much-needed advice and continuous encouragement.

Finally, I would like to thank my committee members Dr. Brenda Bloodgood and Dr. Gulcin Pekkurnaz for their time and support in furthering my education.

ABSTRACT OF THE THESIS

Time- and Circadian-Dependent Fluctuations of Mammalian Nuclear Reorganization

by

Nicolette Marie Allaway

Master of Science in Biology

University of California San Diego, 2019

Professor Mark H. Ellisman, Chair
Professor Brenda Bloodgood, Co-chair

Circadian rhythms coordinate the body to Earth's day and night cycles, relying on sunlight to induce expression of circadian genes which signal downstream and synchronize other tissues. Studies have found that both the positioning of a cellular nucleus, as well as the chromatin organization inside the nucleus, are dynamic to spatially facilitate fluctuating cell functions. Because circadian cycles are rhythmically activating and deactivating genetic material,

the connection between spatial organization of the nucleus and circadian rhythms should be further explored. To study chromatin reorganization and nuclear positioning in the context of circadian rhythms, we used fluorescence and electron microscopy for time-dependent imaging of nuclei of both live mammalian cells and fixed mouse tissue. We measured time-dependent nuclear rotation rates of mouse embryonic fibroblasts (MEFs), human epithelial kidney cells (HEK293Ts), and primary mouse neurons. We used electron microscopy to compare chromatin organization in mouse neurons of the suprachiasmatic nucleus (SCN) between morning, afternoon, and night. Chromatin density analysis of SCN neurons revealed varying condensation patterns of heterochromatin and euchromatin within the nucleus, these data serving as a time-dependent contextual map for distribution of genetic material. In conclusion, these data supply further understanding of how nuclear reorganization may connect to circadian activity. Ultimately, structural data from studies like this can be used together with proteomic and epigenetic data to gain insight into circadian function and how pathologies arise from dysregulation.

# INTRODUCTION

Circadian rhythms are daily behavioral and internal transitions between day and night that are maintained by endogenous clocks in most of the body's cells (Panda et al., 2002). Daily processes such as the sleep/wake cycle, energy expenditure, body temperature, and hormone secretion fluctuate in our tissues due to the oscillating expression of circadian genes (Bollinger and Schibler, 2014). Most living things are entrained to a ~24-hour circadian cycle, hence the term "circadian," Latin for "about a day" (Bollinger and Schibler, 2014). For example, in the human wake cycle the body's systems are dedicated to breaking down molecules to fuel high energy demand (Hastings, 1991). However, as night falls and we transition to sleep, our metabolism slows, core temperature drops about .5 °C, and sleep-inducing melatonin is secreted. By the next morning, the body will start ramping up cortisol levels to prepare for the day (Hastings, 1991). Our schedules are kept by a central timekeeper in the hypothalamus which uses light input to change circadian gene expression and downstream synchronization in peripheral tissues (Jagannath et al., 2017).

Desynchronization of circadian rhythms within the body can have consequences for many aspects of health. Aging, environmental stresses, and insufficient nutrients are all pressures that dysregulate the body's circadian cycles in peripheral tissues (Hastings et al., 2003). Disrupted cycles affect timing and levels of mitosis and metabolic balance, promoting diseases like Alzheimer's, cardiovascular disease, and cancer (Hastings et al., 2003). Additionally, mood disorders such as depression and schizophrenia are associated with abnormal cycles (Christiansen et al., 2016). Due to complete loss of light input, blind people often suffer from circadian dysregulation issues, such as lack of sleep and energy (Sack et al., 2000). The wide range of health issues implicated by irregularities in circadian cycles has motivated research into

the genetic basis of circadian rhythms and disease pathways involved (Hastings et al., 2003). Looking to the future, progress in biological clock research will contribute to the development of drugs and therapies targeting disrupted sleep/wake cycle-related diseases.

Circadian rhythms in humans are controlled by the suprachiasmatic nucleus (SCN), a cluster of ~100,000 neurons on each side of the ventral hypothalamus (Welsh et al., 2010). The SCN is referred to as the circadian pacemaker of the body because the neurons receive light input from the retina and control outputs that synchronize clocks in the rest of the body (Crosio et al., 2000). This pacemaker function has been established through SCN lesion experiments, creating disorganized daily time patterns of drinking and activity on running wheels in lesioned rats (Stephan and Zucker, 1972). The endogenous clock within the SCN is organism-specific and transferable: Tau mutant hamsters with short 20-22-hour circadian periods adopted corrected 24-hour periods after SCN transplants from a wild-type hamster (Ralph et al., 1990). Though light input to the optic nerve is the major environmental trigger of daily cycles, SCN neurons can still maintain rhythmic circadian gene expression when isolated in culture, even without light input (Welsh et al., 2010).

In the neurons of the SCN, major biological clock genes and their proteins make up transcriptional-translational feedback loops which provide the distinction between the day and night cycles (King and Takahashi, 2000). Light signals relayed from the eye cause excitation of SCN neurons, and ultimately control the activity of transcriptional-translational feedback loops through calcium and cAMP influx from light-responsive retinal cells (Lim et al., 2017). The prominent negative feedback loop involves translation of Period (PER) and Cryptochrome

(CRY) proteins during the day which form complexes to inhibit their own transcription at night (Fig. 1).

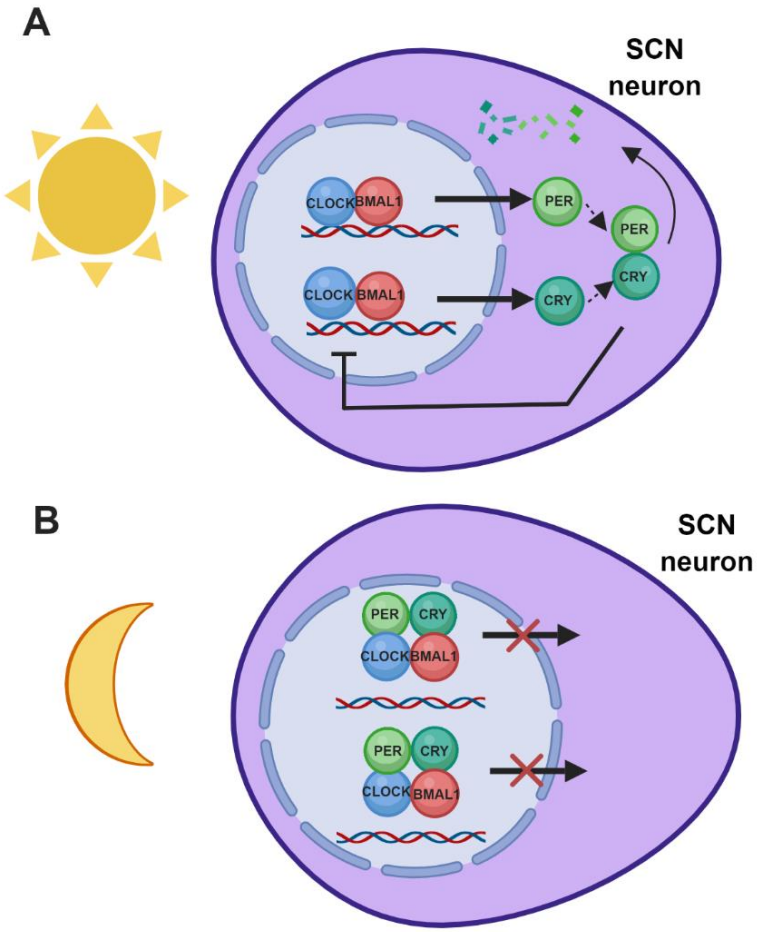


**Figure 1. Negative feedback loop of core clock genes in the SCN neurons. A)** During the day, CLOCK and BMAL1 heterodimers bind to promotors of Per and Cry genes, promoting Per and Cry protein translation. Enzymes degrade Per and Cry in the cell. **B)** At night, PER and CRY complexes return back to the nucleus and bind CLOCK-BMAL1 to inactivate them, subsequently inhibiting Per and Cry transcription. Created with BioRender.com.

Specifically, transcription factors Circadian Locomotor Output Cycles Kaput (CLOCK) and Brain and Muscle ARNT-Like 1 (BMAL1) bind to promotor regions of period (*PER*) and cryptochrome (*CRY*) genes to generate CRY 1 and 2, and PER 1, 2, and 3 proteins. Once translocated outside the nucleus, PER and CRY proteins form a complex in the cytoplasm that reenter the nucleus and bind CLOCK and BMAL1 heterodimers, which inhibits manufacture of

more PER and CRY proteins at night (Lim et al., 2017). This cyclic system sets up the time-dependent day-to-night distinction in SCN neurons and subsequently in peripheral clocks. The PER/CRY feedback loop in conjunction with downstream transcriptional-translational feedback loops synchronize SCN neurons to each other and to oscillators in peripheral tissues, keeping the precise schedule of our rhythmic behaviors (McClung, 2007).

An estimated 82% of protein-coding genes are expressed rhythmically in the body's cells (Mure et al., 2018). At the molecular level, genetic material is therefore structurally changing to accommodate its daily functions. Genetic reorganization of chromatin in the nucleus is dictated by what genes need to be expressed; the dynamic folding of chromatin is liquid-like, activating and deactivating genes, which affects the rates and locations of RNA transcription and DNA activity (Nozaki et al, 2018). It has been determined that spatial organization of genetic material within the nucleus is a coordinated architecture, but the implications of this architecture for cell function is not completely understood. For example, chromosomes exist in spatial domains in the nucleus called chromosome territories, which have been mapped in plants and animals (Cremer & Cremer, 2001). In general, a spatial pattern has been observed in which active genes are decondensed and centralized in the nucleus, while repressed genes reside toward the nuclear periphery as highly condensed heterochromatin (Xu et al., 2018). Nuclear architecture undergoes changes via epigenetic regulation of genes through acetylation, methylation, or phosphorylation of histones, which facilitate DNA decondensation or condensation for steric availability to transcribe proteins (Xu et al., 2018). For example, the CLOCK protein together with its heterodimer BMAL1 act as a histone acetyltransferase (HAT), binding enhancer boxes of PER and CRY genes and enabling chromatin remodeling (Doi et al., 2006). A study investigating the response of mouse SCN neurons to light at night observed chromatin remodeling in SCN

neurons via phosphorylation of histone H3, inducing c-fos and Per1 expression (Crosio et al., 2000). Since most genes appear to be under circadian control, there is an incentive to understand the fluctuating DNA structure and organization of chromosomes inside nuclei, especially in circadian pacemaker neurons of the SCN. Fortunately, advances in electron microscopy and chromatin conformation imaging have enhanced the ability to capture the spatial organization of the nucleus, chromosome territories, and epigenetic modifications of DNA (Xu et al., 2018). DNA and proteins are fixed in transmission electron microscopy sample preparation, providing an enhanced detailed view of chromatin folding inside nuclei of tissues or cultured cells (Bozzola, 2014).

Not only are the internal components of cell nuclei constantly changing to accommodate cell function, but the nucleus as a whole repositions itself via rotation. Rotation of the nucleus is controlled by crosstalk via signaling between the extracellular matrix (ECM) and structural proteins in the cytoskeleton, which reorganizes DNA and affects gene expression (Hay & De Boni, 1991; Wu et al., 2011; Spencer, Xu, & Bissell, 2007). The ECM affects cell shape and its disruption, which can lead to functional instability of the cytoskeleton, a reason for the genetic malfunctions of irregularly-shaped cancer cells (Roskelley, Desprez, & Bissell, 2006). Matrigel® is a gelatinous mixture of ECM proteins, including laminin and collagen, used in cell culture to foster a 3D environment for better cellular support and function (Kleinman & Martin, 2005). Treatment with ECM gel has proven to affect expression of diverse classes of genes such as those involved in metabolic pathways and RNA transport in human mammary epithelial cells, colorectal cancer cells, and hepatocytes (Roskelley, Desprez, & Bissell, 2006; Luca et al., 2013; Page et al., 2007). To test if application of an ECM environment to cells could affect nuclear rotation, we compared nuclear rotation rates of mouse embryonic fibroblasts (MEFs) and human

epithelial kidney cells (HEK293T) cultured with and without Matrigel. Nuclear rotation rates of dorsal root neurons can be manipulated by administering modulators of gene expression such as Nerve Growth Factor or gamma-Aminobutyric acid (GABA) (Fung & De Boni, 1998). Knowing that inducing changes in gene expression affects nuclear rotation rates, we wanted to know if cell nuclei expressing rhythmic circadian genes would rotate faster or slower at different points in the rhythmic cycle. Incubating rat fibroblasts in serum-rich medium induces synchronized rhythmic expression of circadian genes *Rper1*, *Rper2*, *Rev-erbα*, and *Dbp* (Balsalobre et al., 1998). Using the methods of Balsalobre and colleagues, we synchronized circadian expression of MEFs, then measured rotation rates of nuclei at subsequent hours. Studies measuring nuclear rotation over time with respect to circadian rhythms and gene expression may provide mechanistic insights through which chromatin organization by circadian regulation are associated with physical rotation of the nucleus.

This study uses microscopy to relate time and circadian rhythms to both nuclear rotation and nuclear reorganization of chromatin. In Part A, we utilized live-cell fluorescence microscopy to determine nuclear rotation rates of not only human epithelial kidney cells, but also mouse embryonic fibroblasts, as well as primary mouse neurons, and measured how rotation rates change under different culture conditions. To study how circadian rhythms potentially influence spatial organization of DNA in the nucleus, in Part B we performed transmission electron microscopy on thin sections of SCN tissue to compare chromatin organization in SCN neurons between morning, afternoon, and night. Our results add to the discussion of how physical properties of the nucleus dictate cellular function, especially under circadian control.

# MATERIALS AND METHODS

## PART A: Nuclear Rotation of Live Cultured Cells

### Human Embryonic Kidney (HEK293T) Culture

HEK293T cells were plated on 25 $cm^2$ cell culture flasks (Thermo Scientific) and incubated at 37℃ and 5% $CO_2$. Cells were propagated in regular medium containing Dubelcco's Modified Eagle Medium (DMEM) (ThermoFisher Scientific), 10% fetal bovine serum, 1% L-glutamine, and .5% penicillin/streptomycin. Cells at high confluency were diluted by a factor of 1:8 every few days by extraction of the regular medium, a wash with 10 mL phosphate buffered solution, and a short incubation in 1 mL trypsin to detach the cells from the flask. Then 1 mL of the dissociated cells were transferred into a new 25 $cm^2$ flask with 9 mL fresh medium.

### Mouse Embryonic Fibroblast (MEF) Culture

MEF cells were plated on 25 $cm^2$ cell culture flasks (Thermo Scientific) and incubated at 37℃ and 5% $CO_2$. Cells were propagated in regular medium containing Dubelcco's Modified Eagle Medium (DMEM) (ThermoFisher Scientific), 10% tetracycline-free fetal bovine serum, 1% L-glutamine, and .5% penicillin/streptomycin. Cells at high confluency were diluted by a factor of 1:8 every few days by extraction of the regular medium, a wash with 10 mL phosphate buffered solution, and a short incubation in 1 mL trypsin to detach the cells from the flask. After addition of 7 mL medium, the solution was pipetted into a 50 mL conical centrifuge tube and centrifuged for 5 minutes at 1200 revolutions per minute. The supernatant was removed from the centrifuge tube and 9 mL of fresh medium were added to the pellet of MEF cells. After a thorough mixing in the fresh medium, 1 mL of the solution was pipetted into a new 25 $cm^2$ flask with 9 mL fresh medium.

**Mouse Primary Neuron Culture**

Primary dissociated mouse neurons were maintained by incubation at 37℃ and 10% $CO_2$. The neurons were supplemented weekly with regular medium containing Dubelcco's Modified Eagle Medium (DMEM) (ThermoFisher Scientific), 10% fetal bovine serum, 1% L-glutamine, and .5% penicillin/streptomycin.

**Plating on Matrigel Extracellular Matrix**

To provide structural support to cultured cells, a layer of Corning Matrigel Matrix, a hydrogel rich in extracellular matrix proteins laminin and collagen, was used to coat the bottom of MatTek dishes before confocal imaging. This method was achieved by first thawing the Matrigel to 4°C on ice for 2 hours, then 15 μL of the gel was cold pipetted to coat the bottom of dishes to be used on the microscope stage. The dishes were incubated at 37°C for 20 minutes to solidify the gel layer. Next, 200 μL of 50% cell suspension ($3 \times 10^4$ cells)/50% Matrigel was cold pipetted into the dish. About 2 mL of regular medium with 2% Matrigel were pipetted to fill the dish.

**Synchronizing MEF circadian cycles**

Incubation in high-serum medium catalyzes synchronized expression of circadian genes. MEF cells were incubated in 50% FBS/ 50% regular medium for one hour. Following the hour, the medium was returned to regular medium, and cells were placed in imaging medium containing 10 μM DRAQ5 before being transferred to the fluorescence microscope for imaging. The serum-shocked MEF cells were imaged at 10-minute intervals for one or two hours either 2, 6, or 12 hours after the serum shock synchronized the MEFs' circadian rhythms.

**Fluorescence microscopy**

An Olympus Fluoview FV1000 confocal laser scanning microscope was used to visualize DNA-stained nuclei of live HEK293T cells, MEFs, and primary mouse neurons. Live-cell imaging was possible with a temperature-controlled chamber with a $CO_2$ pump to maintain an environment of 37°C and 5% $CO_2$. Image stacks of z-planes were obtained using a 60x objective lens and 3.5x digital magnification with a 633 nm laser to excite DRAQ5. Before transfer to the microscope stage, cultured cells were incubated for 10 minutes in imaging medium made of HBSS, 10% FBS, 10 mM Hepes, and .0025 mM DRAQ5. Live cells were observed and imaged at 10-minute intervals over one or two hours on the confocal microscope.

**Quantitative analysis of nuclear rotation**

Images were analyzed using ImageJ and Photoshop. For rotational rates, location of centers of fluorescent nucleoli or other prominent cell markers were compared against the coordinates of the center of nucleus at each time point using ImageJ coordinate system. Centerpoints of DRAQ5-stained cell markers within the nucleus were measured on an x,y-coordinate plane within ImageJ regarding nuclear center as the origin. The angle of the cell marker with respect to nuclear center was found using tangent calculations with the (x,y) values. Angles of two or three cell markers per each cell were measured from images captured every 10 minutes across one or two hours. Relative degrees of rotation with respect to the center of the nucleus were calculated for a degrees per minute value. To generate data plots in Figures 2-5 rotation values of cell markers were averaged for each cell. Significant rotation in this study is defined as clockwise or counterclockwise movement >1 degree per minute.

## PART B: Chromatin reorganization in the SCN

### Mouse models

Mice (*Mus musculus*) were obtained from the Welsh Lab at the University of California, San Diego. Mice were housed in a 12-hour light/12-hour dark cycle, exposed to light daily from 5 AM to 5 PM.

### Mouse perfusion and brain dissection

Mice were anesthetized with an intraperitoneal injection of 10 mg ketamine, 1 mg xylazine and .0081 mg saline. A tail pinch and paw prick were used to test whether mice were fully anesthetized. Ringer's salt solution of composition .135 M NaCl, 1.27 mM $Na_2HPO_4$, 5.03 mM KCl, .98 mM $MgCl_2 \cdot 6\ H_2O$, and 14.9 mM $NaHCO_3$ with .2 g dextrose was used for the perfusion. The Ringer's solution was placed in a 37°C heat bath while bubbled with 95% air/5% $CO_2$. Before the Ringer's was pumped through the heart to clear the blood, 1 mL .204 M $CaCl_2 \cdot 2\ H_2O$, 1 mL of 1000 units/mL heparin, and 1 mL of 2% xylocaine were added to the warm solution. A peritoneal incision was made for placement of 25-gauge needle into heart. Perfusion of mice was done with a peristaltic pump set to a flow rate of 8-10 mL/min. Following the perfusion of Ringer's solution, a fixative solution of 2% formaldehyde/ 2.5% glutaraldehyde in .15 M cacodylate buffer with 2.04 mM $CaCl_2 \cdot 2\ H_2O$ at 37°C perfused through the mouse for about 10 minutes or until mouse was physically rigid. Once the perfusion with fixative was complete, the brain was dissected and kept refrigerated at 4°C in the fixative solution overnight.

A Leica VT1000s vibratome was used to section the fixed mouse brains into 65 µm thick slices. The brains were sectioned in a cold bath of .15 M cacodylate buffer with 2 mM $CaCl_2$. Slices containing SCN of the hypothalamus were identified using a mouse brain atlas and collected for further processing.

**DRAQ5 DNA-staining and DAB photo-oxidation**

The 65 µm slices were kept on ice and washed 5 x 2 min .15 M cacodylate buffer with 2 mM $CaCl_2$ following vibratome sectioning. They were placed in a quenching buffer of 20 mM glycine in .15 M cacodylate buffer with 2 mM $CaCl_2$ for 5 minutes to quench the unreacted glutaraldehyde. Another set of 5 x 2 min washes in .15 cacodylate buffer with 2 mM $CaCl_2$ was performed after the quenching. To stain the DNA, the slices were placed in 10 µM DRAQ5 (Deep Red Anthraquinone 5) solution for one hour. Excess DRAQ5 was discarded with three washes of .15 M cacodylate buffer with 2 mM $CaCl_2$ after the hour. Once dyed and washed, the samples were exposed to a 3,3'-Diaminobenzidine (DAB) solution for 15 minutes. The DAB solution was prepared as follows: 5.4 mg free base DAB was dissolved in 1 mL of .1 M HCl, then filtered into 9 mL of .15 M cacodylate buffer with 2 mM $CaCl_2$. The 65 µm brain slices were transferred into a glass bottom MatTek dish containing the freshly made DAB solution for at least 15 minutes. After the DAB solution properly infiltrated the samples, they were transferred to the 4°C cold stage of a confocal Leica SPE II confocal microscope with an oil immersion 63x objective lens. A 635 nm laser was used to excite the DRAQ5, which catalyzes the polymerization of DAB onto DNA. For each brain slice, both SCN clusters on either side of the third ventricle were photo-oxidized by continuous fluorescent illumination for 5-20 minutes. The photo-oxidation process creates a visual darkening of the nucleus as DAB polymerizes on chromatin, which causes the fluorescence signal from DRAQ5 to fade during the reaction. The samples were monitored for changes in color and fluorescence signal, and the reaction was halted by replacing DAB solution with three washes of .15 M cacodylate buffer. Samples were returned to ice baths after photo-oxidation on the microscope.

**Electron microscopy sample preparation and TEM**

Following photo-oxidation, the region of interest was cut out of each slice with a razorblade. For one hour, the samples were placed in reduced $OsO_4$, made by combining equal volumes of 4% $OsO_4$ in water with 3% potassium ferrocyanide in .3 M cacodylate buffer. The osmium was washed out with double distilled water 3 x 5 min, followed by overnight refrigeration in 2% filtered uranyl acetate. The next morning the uranyl acetate was rinsed three times with double distilled $H_2O$. The samples were transferred from dishes to glass scintillation vials on ice, then successively dehydrated in ethanol for 10 minutes each in cold 50%, 70%, 90% ethanol, then 10 minutes each in room temperature 100% ethanol twice, 50% ethanol/50% acetone, and 100% acetone twice. Durcupan epoxy resin was made using a component A:B:C:D ratio of 11.4 g: 10 g: .3 g: .1 g. Following the dehydration, the samples were placed in 50% acetone/ 50% resin for 2-4 hours or overnight. The samples were then transferred into aluminum tins containing fresh resin for 24 hours. A second 24 hours in fresh resin was followed by a third resin treatment for at least 3 hours. The samples were mounted flat between mold-release glass slides filled with resin and incubated in a 60°C oven for 48 hours.

The slides were removed from the oven and the embedded samples were carefully cut in half and glued on plastic blocks, so each block held one side of the SCN. The blocks were trimmed and sectioned with a diamond knife into 70 nm slices using a Leica Ultracut UCT ultramicrotome. The slices were collected on copper mesh grids and imaged at 80 kV with a FEI Tecnai transmission electron microscope at 3200x or 2700x magnification, with exposure time 1 second.

**Chromatin Organization Analysis**

The images of SCN nuclei that were collected were analyzed to measure chromatin concentration as a function of distance from the nuclear periphery. TEM images of nuclei were traced along the nuclear membrane using 3dmod image processor. A custom analysis script in Matlab was used classify chromatin density. Therefore, the Otsu algorithm (Otsu, 1979) was applied within the traced region on a one to four scale, four being the highest concentration. The scale was created based on pixel intensity from the traced TEM images. The traced regions were divided into 100 nm thick radial layers, and each layer was given an averaged chromatin density score. Neurons from 10 AM, 3 PM, and 8 PM were scored per layer and averaged into one set of values for each time group to give a plotted chromatin density score as a function of distance from the nuclear membrane.

# RESULTS

## Part A: Nuclear Rotation of Live Cultured Cells

In order to get an understanding of the basic dynamics in nuclear organization, we wanted to compare rotational rates of nuclei in three cell types under varied conditions. Live-cell imaging experiments were performed to image DNA-stained nuclei at 10-minute intervals. The images were processed and compared against each other to follow the rotation of each nucleus over time. It has been established that the nuclear envelope is important for maintaining the organization of the nucleoplasmic contents, including chromatin (Zuleger et al., 2011). It is implied that nuclear rotation, and therefore rotation of the nuclear envelope, is important for cell functioning, as chromatin reorganizes to facilitate gene expression and repression.

### Human Epithelial Kidney Cells

HEK293Ts were imaged in vitro and observed for possible nuclear rotation. Figure 2 plots the nuclear rotation of HEK293T nuclei over time. The mean total rotation of all HEK293Ts (N=10) was 228.7 degrees per hour and mean net rotation was 85.5 degrees per hour. Additional experiments were performed on cells grown on Matrigel-coated culture plates to see if rotation rates would be affected by the addition of ECM components. Cells without Matrigel appeared more stationary than those with Matrigel. However, a student's t-test determined there was no significant difference between rotation rates (degrees/min) of HEK293Ts on Matrigel (M=.90, SD=1.30) and HEK293Ts without Matrigel (M=.67, SD=.32), $t(10)= -.448$, $p= .05$.

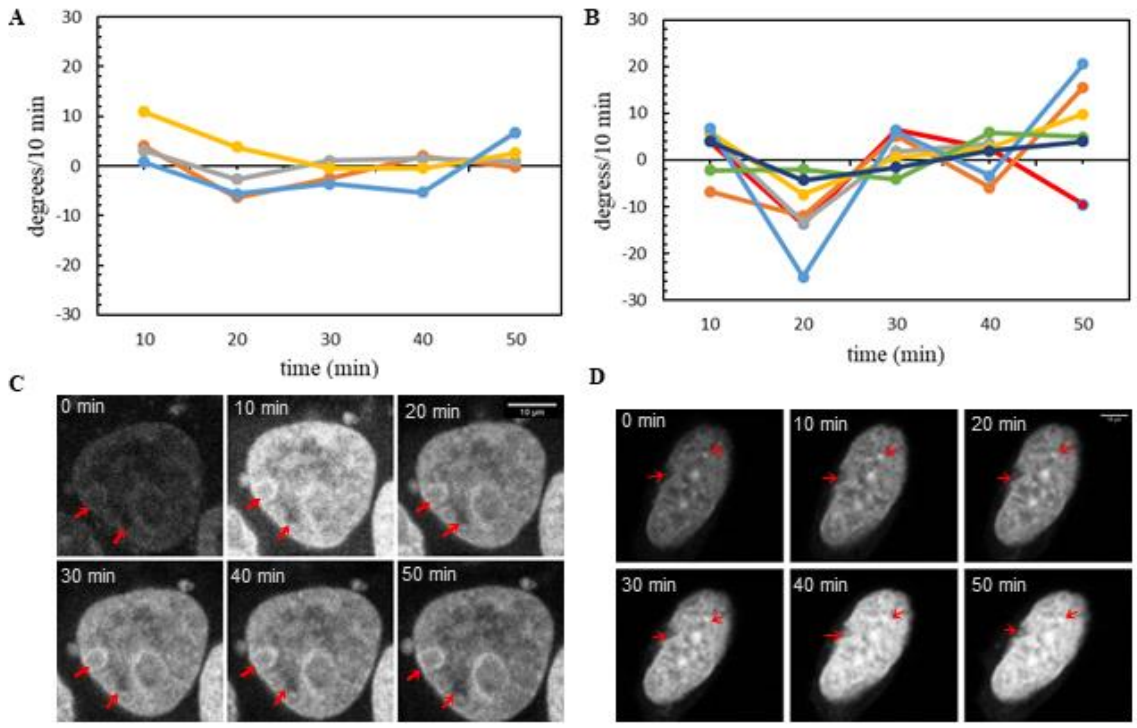


**Figure 2. Nuclear rotation of DNA-stained HEK293Ts with and without Matrigel.** Comparison of nuclear rotation rates of HEK293Ts in **A)** regular culture conditions (N=4, mean= .67 ± .32 º/min) and **B)** cultured with Matrigel (N=7, mean= .90± 1.30 º/min). Each colored line represents one nucleus, using averaged values from two or three cell markers inside each nucleus. Negative y-values indicate clockwise rotation, positive y-values indicate counterclockwise rotation. **C)** Fluorescence signal of HEK293T nucleus in regular culture conditions represented by the orange line in (A). **D)** Fluorescence signal of HEK293T nucleus cultured with Matrigel represented by the red line in (B). Data was plotted from averaged values of the cell markers indicated by red arrows. Scale bars are 10 μm.

**Mouse Embryonic Fibroblasts**

Next, another cell type, MEFs, were imaged under the same conditions, both with and without plating on Matrigel. Figure 3 displays plotted values for nuclear rotation of MEFs under these two conditions. The MEF nuclei with Matrigel displayed more dramatic rotation in both clockwise and counterclockwise directions than the MEFs without Matrigel. A student's t-test determined there was a significant difference between rotation rates (degrees/minute) of MEFs on Matrigel ($M=1.06$, $SD=.61$) and MEFs without Matrigel ($M=.20$, $SD=.16$); $t(11)=3.29$, $p=.05$.

To test if nuclear rotation could be associated with a circadian component, we induced synchronized cyclic expression of circadian genes through a high serum treatment (Balsalobre et al., 1998). Time lapsed fluorescent images of DNA-stained MEFs were captured beginning either 2, 6, or 12 hours after the treatment. Figure 4 shows plotted angle changes of cell markers in the nucleus across 1 or 2 hours for each time group. A one-way ANOVA test found a significant time-dependent effect on rotation rates between the 2-, 6-, and 12-hour groups at the $p< .10$ level [$F(2,12)=3.27$, $p= .074$]. As plotted in Figure 4, MEF cells were found to rotate the most 12 hours post-shock and less dramatically 6 hours post-shock. Rotation rates for 2 hours post-shock were lower than both 6 and 12 hour measurements.

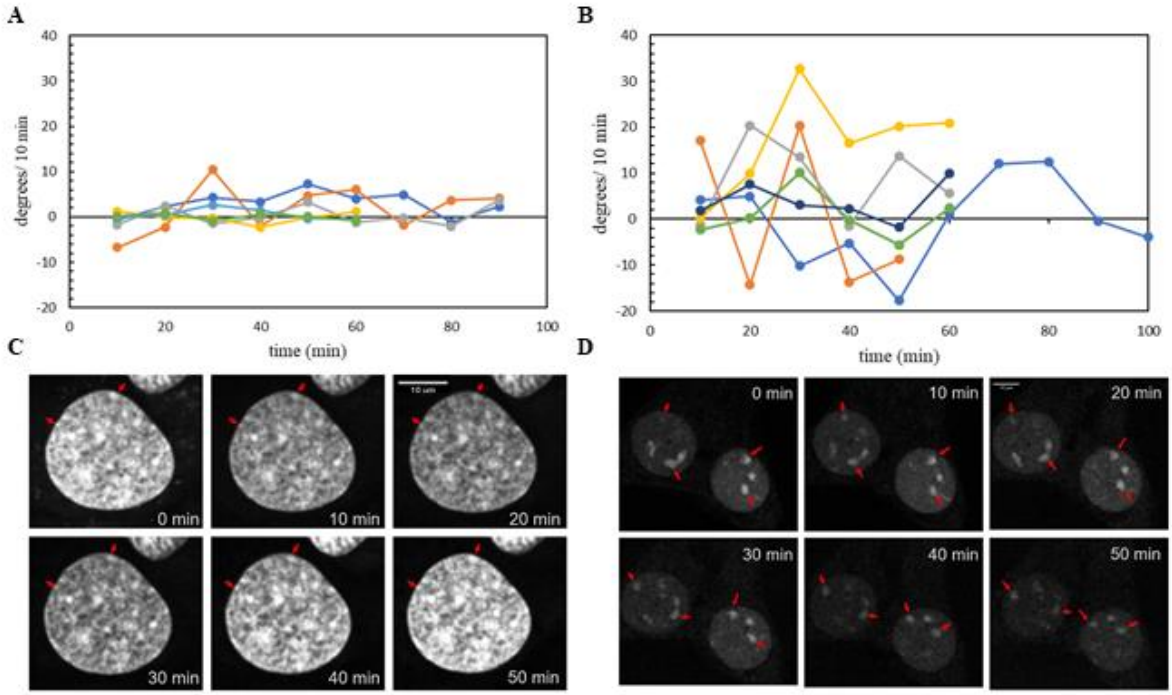


**Figure 3. Nuclear rotation of DNA-stained MEFs is faster on Matrigel.** Comparison of nuclear rotation rates of MEFs in **A)** normal culture conditions (N=6, mean=1.06± .61 º/min) and **B)** cultured on Matrigel (N=6, mean= .20 ± .16 º/min). Each colored line represents one nucleus, using averaged rotation values from two or three cell markers inside each nucleus. Negative y-values indicate clockwise rotation, positive y-values indicate counterclockwise rotation. **C)** Fluorescence signal of MEF nucleus in regular culture conditions represented by the green plotted line in (A). Data was plotted from averaged values of cell markers indicated by red arrows. **D)** Fluorescence signal of two MEF nuclei cultured with Matrigel represented by the yellow and gray plotted lines in (B). Data was plotted from averaged values of cell markers indicated by red arrows. Scale bars are 10 μm.

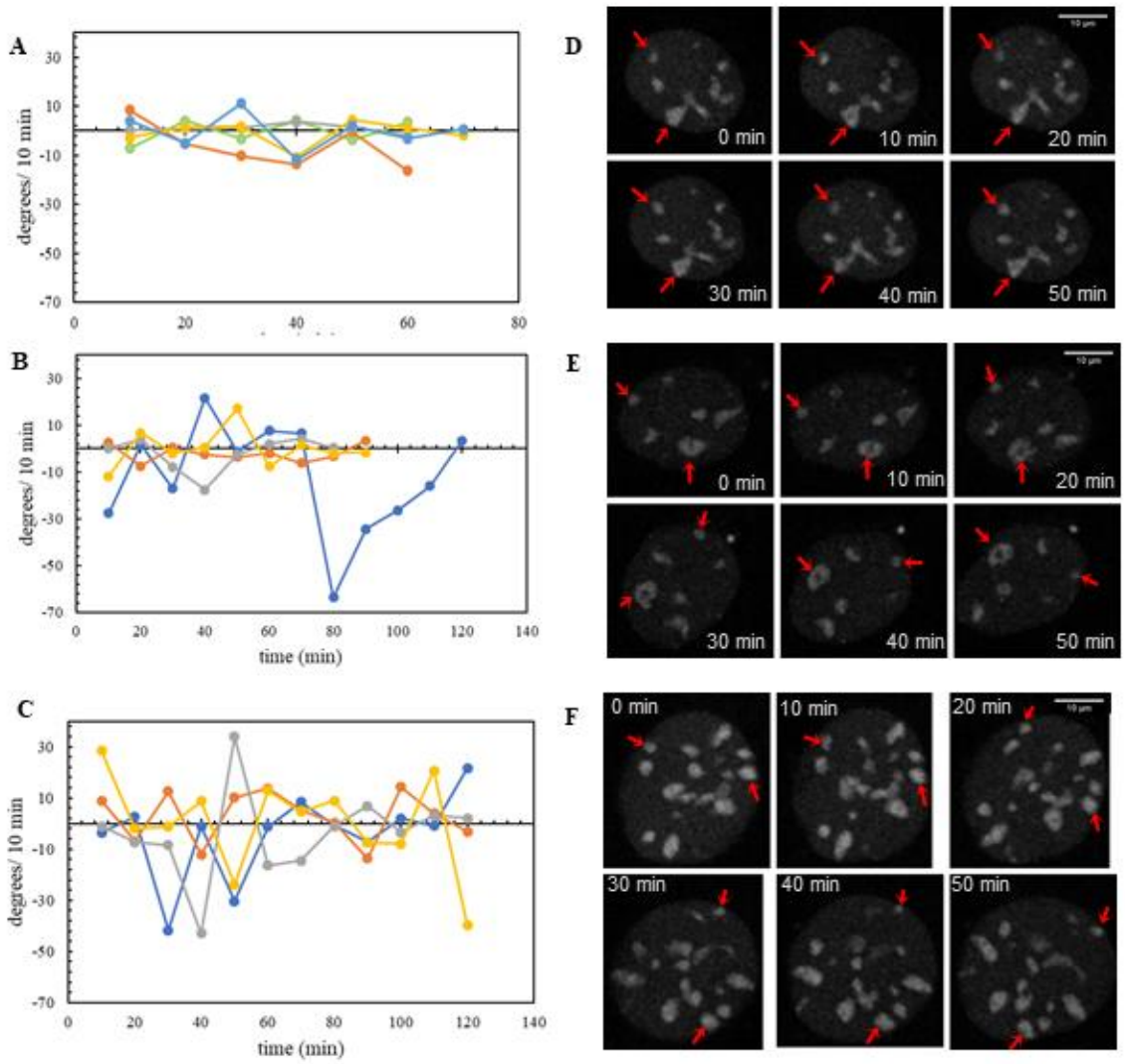


**Figure 4. Circadian-dependent nuclear rotation rates of synchronized MEFs.** Serum-induced rhythmic circadian gene expression in MEF cells produced significantly different nuclear rotation rates beginning at **A)** 2 hours (N=5, mean= .47 ± .28 º/min) **B)** 6 hours (N=4, mean= .85 ± .63 º/min) and **C)** 12 hours (N=4, mean= 1.14 ± .20 º/min) after induction. Each colored line indicates averaged rotation values from two fluorescent cell markers inside one nucleus. Negative y-values indicate clockwise rotation, positive y-values indicate counterclockwise rotation. **D)** Fluorescence signal of MEF nucleus represented by the yellow plotted line in (A). **E)** Fluorescence signal of MEF nucleus represented by the blue plotted line in (B). **F)** Fluorescence signal of MEF nucleus represented by the blue plotted line in (C). Data was plotted from averaged values of cell markers indicated by red arrows. Scale bars are 10 μm.

**Primary Dissociated Mouse Neurons**

DNA-stained primary dissociated mouse neurons were observed over an hour in the same manner as HEK293Ts and MEFs (Fig. 5). Of six neurons measured, none of the nuclei changed orientation significantly: the average net rotation was 6.9 degrees per hour. Figure 5b shows a representative time-lapse fluorescence signal of one neuron, in which the large nucleolus on the periphery was the cell marker used for rotation calculations. The composite of the bright field and fluorescence signal images for the neuron is displayed in Fig. 5C.

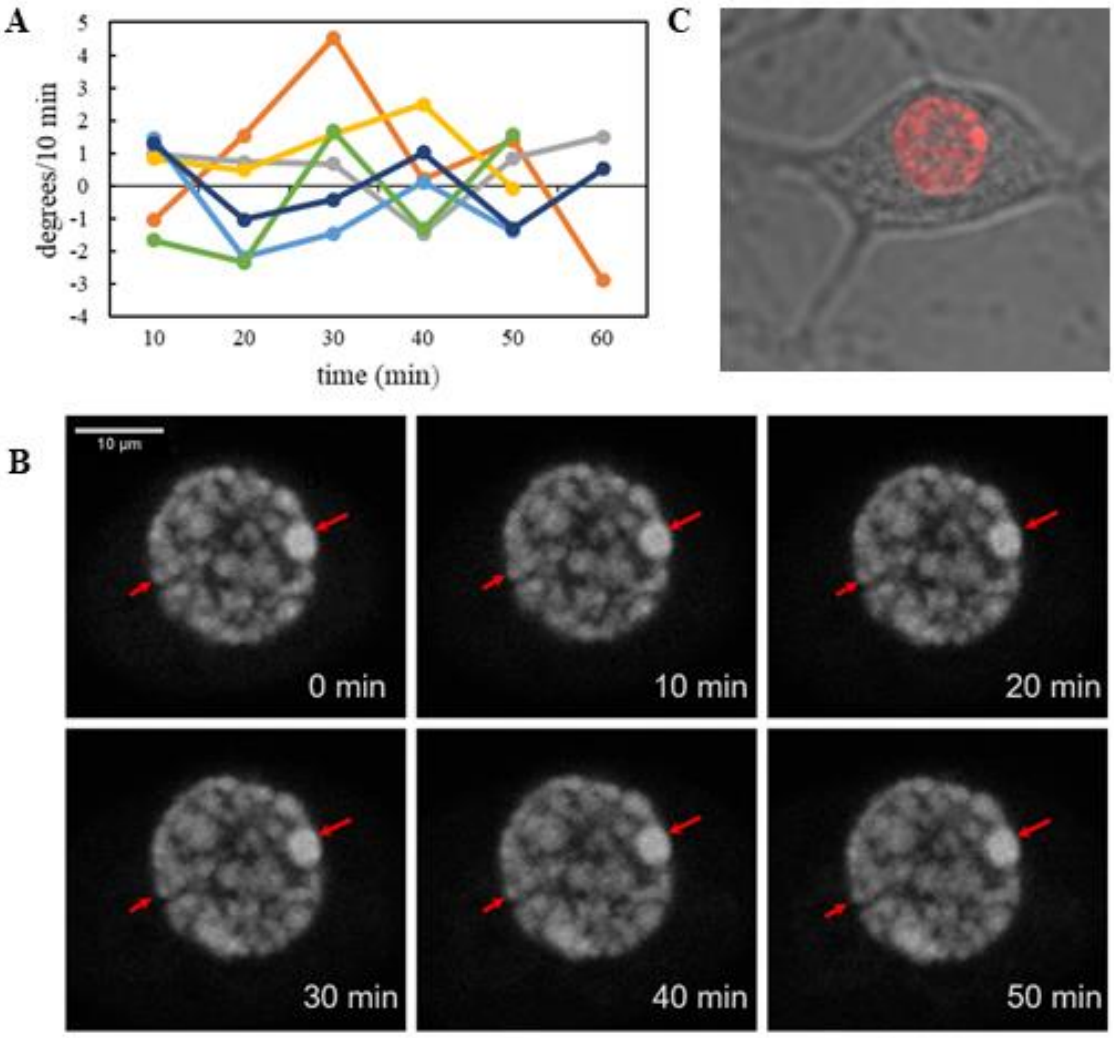


**Figure 5. Primary dissociated mouse neurons exhibit minimal nuclear rotation over time. A)** Rotation of neuronal nuclei (N=6) across one hour. Each colored line represents one nucleus, using averaged values from two cell markers inside each nucleus. Negative y-values indicate clockwise rotation, positive y-values indicate counterclockwise rotation. **B)** Time-lapsed fluorescence signal of neuron nucleus represented by the dark blue line in (A). Data was plotted from averaged values of cell markers indicated by red arrows. **C)** Merged brightfield and fluorescence images of neuron represented by the dark blue line in (A). Scale bars are 10 µm.

**Part B: Chromatin Reorganization in the SCN**

To further investigate the relationship between time and spatial reorganization of the nucleus, electron microscopy was used to image DNA-stained nuclei of mouse SCN neurons fixed in the morning, afternoon, and night. SCN tissue from mice on a 12-hour day/12-hour night cycle was fixed at 10 AM, 3 PM, and 8 PM. Since circadian gene expression is oscillating throughout the day, we wanted to see how chromatin inside nuclei rearranges throughout the day in pacemaker neurons, which express oscillating levels of core clock genes. Chromatin visualization was possible by photo-oxidation of DRAQ5 to catalyze the polymerization of DAB onto chromatin, which forms a dark precipitate visible with electron microscopy (Fig. 6A). The formation of precipitate in the SCN regions of the brain samples was visible under a light microscope (Fig. 6B). Imaging revealed various degrees of chromatin condensation within the nuclei of the neurons, identified by scattered dark clusters of different sizes near the nuclear membrane and throughout the central nucleus. Chromatin condensation was quantified using an algorithm to classify pixel intensity from light to dark, scored on a 1-4 scale (Fig. 7C). The scores were averaged for each 100 nm layer radially inward from the nuclear membrane classified in Figure 7B. Averaged chromatin density values for each neuron captured were averaged across the three mice in each time group to provide a plottable score for 10 AM, 3 PM, and 8 PM neurons (Fig. 8). For each group chromatin density was highest at the nuclear periphery and displayed a sharp drop off until .3 microns away from the membrane. Of the three groups, 10 AM and 8 PM were the most different, and 10 AM consistently contained the lowest chromatin density further away from nuclear membrane, even though 10 AM neurons are denser than 3 PM neurons at the periphery. At the periphery, 8 PM neurons contain the highest density

score and closely match the density inside 3 PM neurons but maintain slightly higher scores throughout the nucleus.

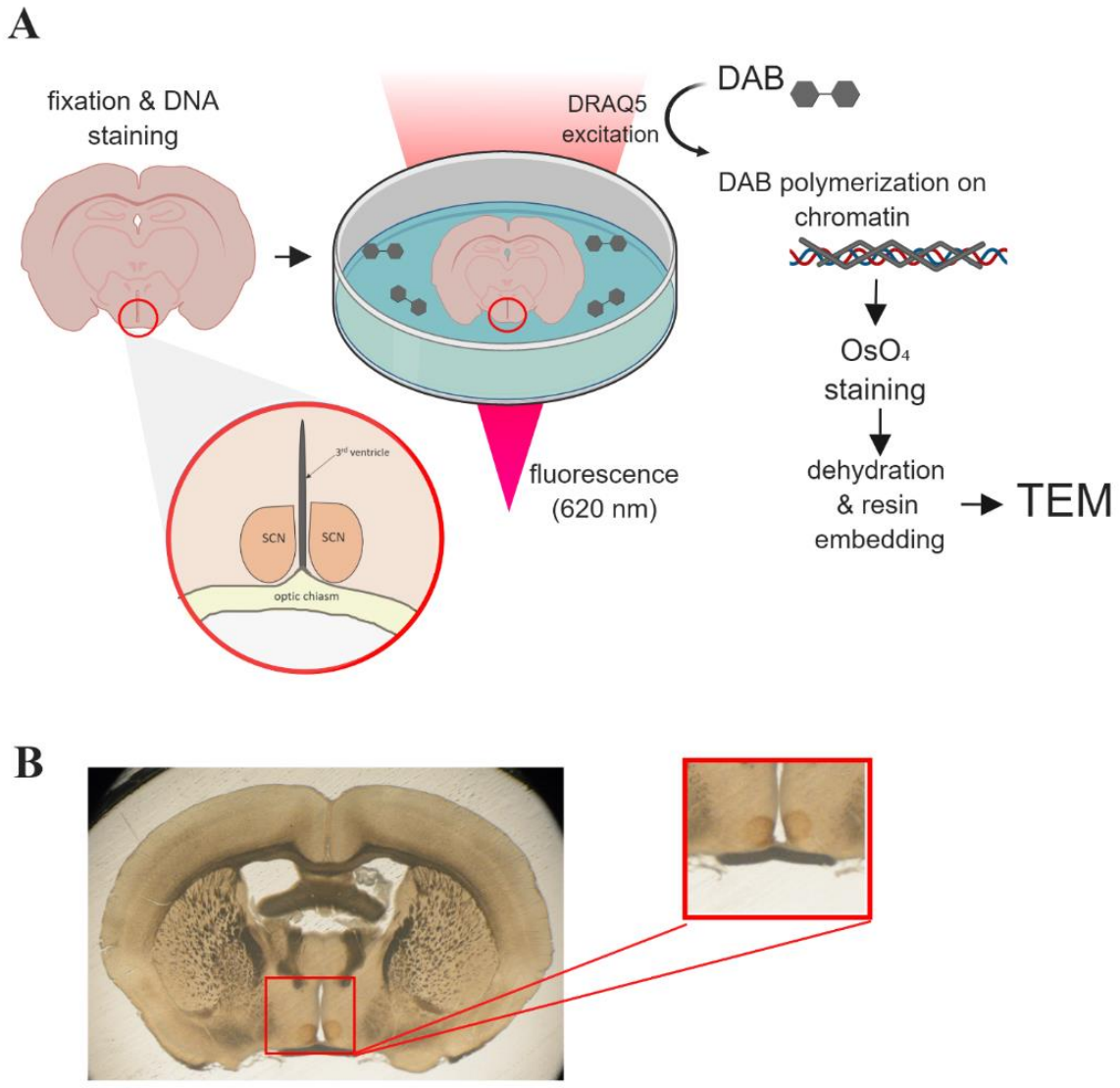


**Figure 6. Preparation of SCN tissue for electron microscopy. A)** DRAQ5-stained, fixed brain slices were photo-oxidized in the SCN region with a far-red laser, causing DAB to polymerize on chromatin for better visualization of DNA. To follow, an osmium treatment for staining lipids, dehydration in ethanol, and embedding in epoxy resin prepared samples for transmission electron microscopy of SCN neurons. **B)** 65 µm brain slice following photo-oxidation of both sides of SCN. The magnified was excised and processed for TEM. The two darkened circles indicate areas of photo-oxidation from laser excitation. Created with BioRender.com

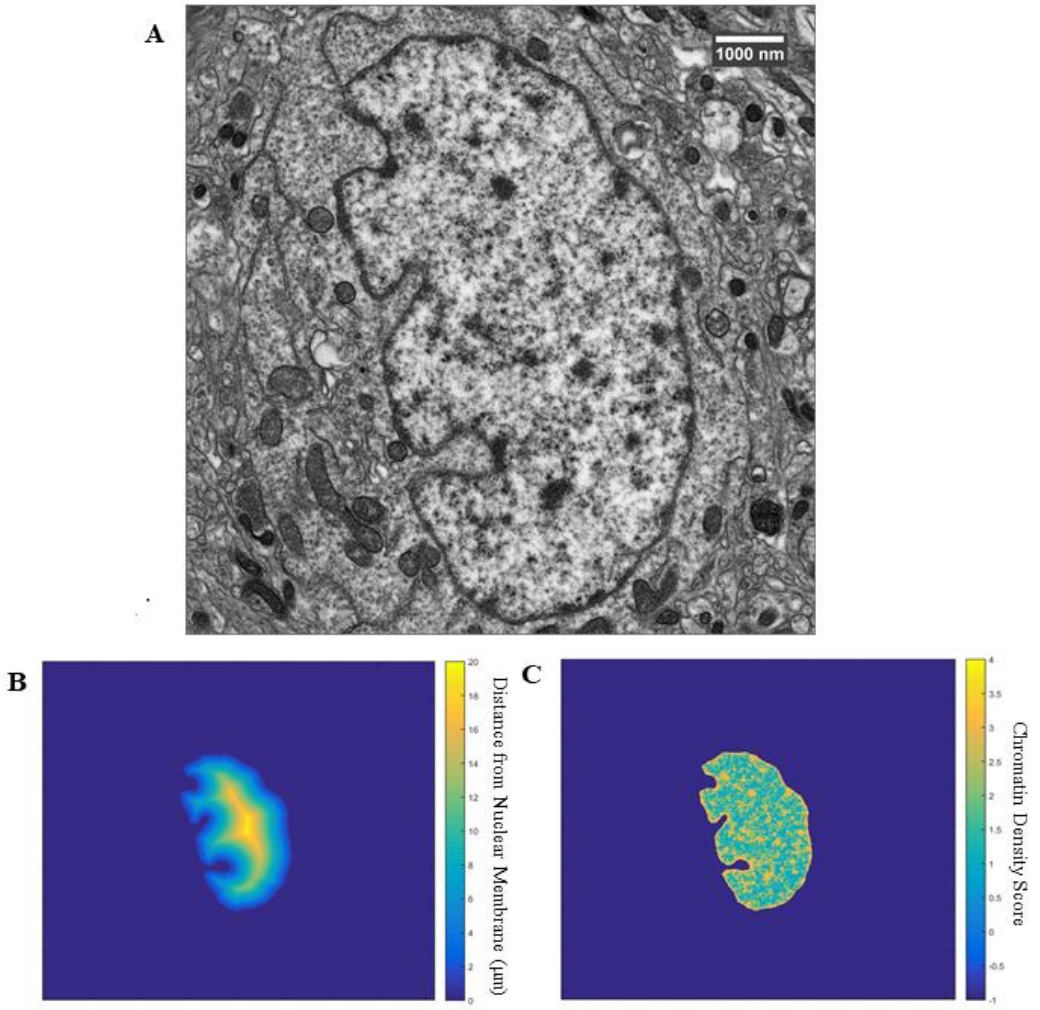


**Figure 7. Chromatin density analysis of SCN neuron from 10 AM. A)** Nucleus of SCN neuron at 2700x magnification. **B)** Division of the nucleus into 100 nm radially inward layers. **C)** Chromatin density score of genetic material inside the nucleus measured by pixel intensity from the image in (A). Density is scored from lowest to highest from 1-4, and -1 indicates excluded area. Scale bar is 1000 nm.

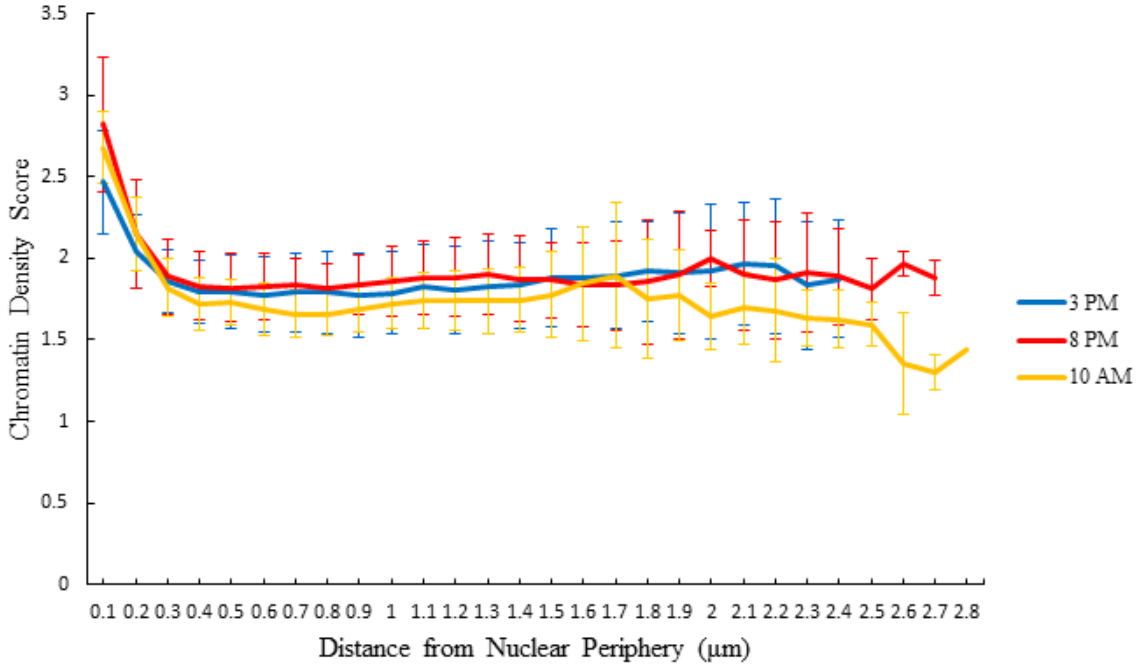


**Figure 8. Chromatin density in SCN neuron nuclei as a function of distance from nuclear periphery between morning, afternoon, and night.** The values were obtained from averaged values of individual neurons in mice from each group, for each time group N=3 mice, totaling 15-20 cells per group. Chromatin density score is valued low to high from 1-4, based on pixel intensity value from each image of nuclei obtained. Error bars represent standard deviation of chromatin density scores in neurons from mice in each time group.

# DISCUSSION

The overarching goal of the experiments in this study was to better understand how activity of the nucleus changes over time and which factors influence this dynamic process. We observed differences in rotation rates of cultured cells both by application of ECM proteins and by inducing circadian gene expression with serum. We also observed the differences in chromatin organization in nuclei of circadian pacemaker neurons between morning, afternoon, and night.

Nuclear positioning and its dynamic changes likely support cell function, such as the changes of activity across time. Even though nuclear rotation has been discovered more than 6 decades ago (Pomerat, 1953), not many studies have quantified nuclear rotation. However, rotation of primary neurons has been manipulated by gene expression modulators (Fung & De Boni, 1988). We hypothesized that since Matrigel provides a structural support around the cells, which helps cells to grow more into tissue-like 3-dimensional cells, that it would result in an increased rotation in cultured cells. A significant effect was seen in MEFs, but not HEK293Ts. Differences in gene expression in human hepatocytes cultured with or without Matrigel matrix have been reported; the hepatocytes with Matrigel expressed down regulation of cytoskeletal, actin binding, and stress response genes (Page et al., 2007). The authors suggested that Matrigel rescues cultured cells from a stressed morphologic state, expressing more *in vivo*-like gene profiles, which supports the hypothesis that Matrigel could have facilitated more rotation of the cultured MEF and HEK293T cells in this study (Page et al., 2007). Our data highlight the importance of nuclear structure for cell activity and suggest that results of *in vitro* assays of cultured cells may be influenced by the extracellular environment provided to the cells.

The goal of measuring rotation of time-synchronized MEF cells was to study whether a connection exists between circadian time and spatial orientation of the nucleus. Earlier studies revealed through measurements of mRNA accumulation of *Rper1*, *Rper2*, *Rev-erbα*, and *Dbp* for 72 hours after serum shock application to rat fibroblasts a ~23-hour circadian period, with minimum expression every 12th hour and peak expression every 23rd hour of the period (Balsalobre et al., 1998). From these expression patterns, we hypothesized that because genetic material is reorganizing that the positioning of the nucleus would change throughout the induced circadian period. Data from experiments in this study support this hypothesis, displaying successively more pronounced rotation rates in MEFs up to 12 hours after a high serum treatment.

Chromatin density of SCN neurons decreased as distance from the periphery increased, with 10 AM neurons containing the least dense chromatin at the center of the nucleus. As expected, condensed heterochromatin gathered at the periphery while less condensed, presumably more active euchromatin was in the center at all time points. We expected to see different proportions of chromatin condensation between time groups, as different sets of genes are turned on and off throughout the day. Our data from each group of morning, afternoon, and night neurons support this expectation and suggest that DNA distribution in the nucleus is fluctuating throughout the day. If the observed differences in DNA distribution were indeed a product of circadian control, this finding provides a potential additionally important link between circadian dysregulation and deficits in gene expression in wide varieties of diseases.

The data in this study are subject to some limitations. We have conducted two-dimensional analyses of rotation of live cells and chromatin organization in single planes of SCN nuclei. Three-dimensional reconstructions of volumetric EM data could provide a complete

spatial map of each nucleus and more insight on how DNA interacts with nucleoplasmic contents. Staining for chromosome territories could add information of how they interact and shift throughout the circadian period. Similarly, the live-cell chromatin analysis of nuclei from this study was conducted in 2D, which does not provide a full picture of how chromatin is spatially re-organized in all three dimensions over time. In addition, three-dimensional analysis of nuclear rotation of live cells could help us determine if cells have a time-dependent preferred spatial polarity or orientation, especially if it were to be combined with subsequent fluorescence in situ hybridization (FISH), or chromosome painting. However, it should be noted that not all strongly stained chromatin areas, which were used to track nuclear rotation, stayed visible throughout the experiments and cells in which less than two markers could be tracked over the entire time had to be discarded (~50% of the cells). To perform 3D rotational analysis, a much larger proportion of the imaged cells would not have sufficient markers.

It is further important to consider that cells in a dish are not necessarily behaving as they would as part of a tissue in the body. Because of this, the lack of structural support from neighboring cells may have affected the shape or physical behavior of the nuclei measured. We tried to mimic the effects of tissue through culturing cell in Matrigel, so measurements in tissue cultures would provide us insights which are closer to the situation *in vivo*. An interesting experiment would be to perform live imaging of nuclear rotation on SCN explants (Wray, Castel, and Gainer, 1993), which would allow us to test the relative contribution of nuclear rotation and the dynamics of re-organization of chromatin condensation with the high resolution of our EM results.

Looking to the future, the connection between circadian rhythms and nuclear organization could be further explored through applying experimental conditions to cells or

animals, such as knockout of core clock genes, manipulation of sleeping or light schedules, or melatonin supplementation. Sleep is a major component of an organism's circadian cycle, yet the function of sleep remains not fully understood. Studying circadian-related chromatin dynamics can possibly answer questions about the function of sleep. Recent work has followed chromosome movement over time in zebrafish neurons and found that chromosomes are more dynamic during sleep (Zada et al., 2019). The authors propose sleep has a restorative function to fix double-stranded DNA breaks that accumulate from daily activities (Zada et al., 2019). Studying chromatin dynamics in live cells in a circadian context may elucidate more differences between DNA distribution between sleep and wake cycles to uncover more about the function of sleep and DNA components involved. Additionally, chromatin condensation maps, such as those in Figures 7 and 8, could be useful in classifying cell types within a tissue or comparing DNA distribution between healthy and disease states to identify abnormalities.

In summary, our time-dependent assessments of mammalian nuclei imply that the dynamic cell functions are carried out by the physical reorganization of the nucleus and its contents. Though studies often turn to the transcriptome for answers about cell function, these answers may lie in studying the nucleus itself as a physical structure. As cell shape, rotation, and chromatin organization can be indicators of genetic malfunctions in disease states, we can look to the physical properties of the nucleus for insight.

REFERENCES


Balsalobre, A., Damiola, F., & Schibler, U. (1998). A serum shock induces circadian gene expression in mammalian tissue culture cells. *Cell*, *93*(6), 929–937.

Bollinger, T., & Schibler, U. (2014). Circadian rhythms - From genes to physiology and disease. *Swiss Medical Weekly*, *144*(July), 1–11.

Bozzola, J. J. (2014). Conventional Specimen Preparation Techniques for Transmission Electron Microscopy of Cultured Cells. In J. Kuo (Ed.), *Electron Microscopy: Methods and Protocols* (pp. 1–19). Totowa, NJ: Humana Press.

Christiansen, S. L., Bouzinova, E. V., Fahrenkrug, J., & Wiborg, O. (2016). Altered expression pattern of clock genes in a rat model of depression. *International Journal of Neuropsychopharmacology*, *19*(11), 1-13.

Cremer, T., & Cremer, C. (2001). Chromosome territories, nuclear architecture and gene regulation in mammalian cells. *Nature Reviews Genetics*, *2*(4), 292–301.

Crosio, C., Cermakian, N., Allis, C. D., & Sassone-Corsi, P. (2000). Light induces chromatin modification in cells of the mammalian circadian clock. *Nature Neuroscience*, *3*(12), 1241–1247.

Doi, M., Hirayama, J., & Sassone-Corsi, P. (2006). Circadian Regulator CLOCK Is a Histone Acetyltransferase. *Cell*, *125*(3), 497–508.

Fung, L. C., & De Boni, U. (1988). Modulation of nuclear rotation in neuronal interphase nuclei by nerve growth factor, by γ-aminobutyric acid, and by changes in intracellular calcium. *Cell Motility and the Cytoskeleton*, *10*(3), 363–373.

Hastings, M. H. (1991). Neuroendocrine rhythms. *Pharmacology & Therapeutics*, *50*(1), 35–71.

Hastings, M. H., Reddy, A. B., & Maywood, E. S. (2003). A clockwork web: Circadian timing in brain and periphery, in health and disease. *Nature Reviews Neuroscience*, *4*(8), 649–661.

He, S., Dunn, K. L., Espino, P. S., Drobic, B., Li, L., Yu, J., Sun, J.M., Chen, H.Y., Pritchard, S., Davie, J. R. (2008). Chromatin organization and nuclear microenvironments in cancer cells. *Journal of Cellular Biochemistry*, *104*(6), 2004–2015.

King, D. P., & Takahashi, J. S. (2000). Molecular genetics of circadian rhythms in mammals. *Annual Review of Neuroscience*, *23*, 713–742.

Kleinman, H. K., & Martin, G. R. (2005). Matrigel: basement membrane matrix with biological activity. *Seminars in Cancer Biology*, *15*(5), 378–386.

Lim, M., Tu, C., Noguchi, T., & Golden, S.S. (2017, June 15). *Common clock mechanism graphics tool*. Retrieved from http://ccb.ucsd.edu/_files/bioclock/projects-2017/clockmechanismgraphicstool_v1.0.pptx.

Luca, A. C., Mersch, S., Deenen, R., Schmidt, S., Messner, I., Schäfer, K. L., Baldus, S., Huckenbeck, W., Piekorz, R., Knoefel, W., Krieg A Stoecklein, N. H. (2013). Impact of the 3D Microenvironment on Phenotype, Gene Expression, and EGFR Inhibition of Colorectal Cancer Cell Lines. *PLoS ONE*, *8*(3), e59689.

Maninová, M., Iwanicki, M. P., & Vomastek, T. (2014). Emerging role for nuclear rotation and orientation in cell migration. *Cell Adhesion and Migration*, *8*(1), 42–48.

McClung, C. A. (2007) Circadian genes, rhythms and the biology of mood disorders. *Pharmacology & Therapeutics*, 114 (2), 222-232.

Mure, L. S., Le, H. D., Benegiamo, G., Chang, M. W., Rios, L., Jillani, N., Ngotho, M., Kariuki, T., Dkhissi-Benyahya, O., Cooper, H.M., Panda, S. (2018). Diurnal transcriptome atlas of a primate across major neural and peripheral tissues. *Science*, *359*(6381).

Nozaki, T., Hudson, D. F., Tamura, S., & Maeshima, K. (2018). Dynamic Chromatin Folding in the Cell. In *Nuclear Architecture and Dynamics* (pp. 101–122).

Ou, H. D., Phan, S., Deerinck, T. J., Thor, A., Ellisman, M. H., & O'Shea, C. C. (2017). ChromEMT: Visualizing 3D chromatin structure and compaction in interphase and mitotic cells. *Science*, *357*(6349).

Otsu, N. (1979). A Threshold Selection Method from Gray-Level Histograms. *IEEE Transactions on Systems, Man, and Cybernetics*, *9*(1), 62–66.

Pomerat, C. M. (1953). Rotating nuclei in tissue cultures of adult human nasal mucosa. *Experimental Cell Research*, *5*(1), 191–196.

Roskelley, C. D., Desprez, P. Y., & Bissell, M. J. (2006). Extracellular matrix-dependent tissue-specific gene expression in mammary epithelial cells requires both physical and biochemical signal transduction. *Proceedings of the National Academy of Sciences*, *91*(26), 12378–12382.

Spencer, V. A., Xu, R., & Bissell, M. J. (2007). Extracellular Matrix, Nuclear and Chromatin Structure, and Gene Expression in Normal Tissues and Malignant Tumors: A Work in Progress. *Advances in Cancer Research*, *97*(6), 275–294.

Stephan, F. K., & Zucker, I. (1972). Circadian Rhythms in Drinking Behavior and Locomotor Activity of Rats Are Eliminated by Hypothalamic Lesions. *Proceedings of the National Academy of Sciences*, *69*(6), 1583–1586.

Weaver, A. M., Hussaini, I. M., Mazar, A., Henkin, J., & Gonias, S. L. (1997). Embryonic fibroblasts that are genetically deficient in low density lipoprotein receptor-related protein demonstrate increased activity of the urokinase receptor system and accelerated migration on vitronectin. *Journal of Biological Chemistry*, *272*(22), 14372–14379.

Webster, M., Witkin, K. L., & Cohen-Fix, O. (2009). Sizing up the nucleus: nuclear shape, size and nuclear-envelope assembly. *Journal of Cell Science*, *122*(10), 1477–1486.

Welsh, D. K., Takahashi, J. S., & Kay, S. A. (2010). Suprachiasmatic Nucleus: Cell Autonomy and Network Properties. *Annual Review of Physiology*, *72*(1), 551–577.

Wray, S., Castel, M., & Gainer, H. (1993). Characterization of the suprachiasmatic nucleus in organotypic slice explant cultures. *Microscopy Research and Technique*, *25*(1), 46–60.

Wu, J., Lee, K. C., Dickinson, R. B., & Lele, T. P. (2011). How dynein and microtubules rotate the nucleus. *Journal of Cellular Physiology*, *226*(10), 2666–2674.

Xu, J., Ma, H., Jin, J., Uttam, S., Fu, R., Huang, Y., & Liu, Y. (2018). Super-Resolution Imaging of Higher-Order Chromatin Structures at Different Epigenomic States in Single Mammalian Cells. *Cell Reports*, *24*(4), 873–882.

Zada, D., Bronshtein, I., Lerer-Goldshtein, T., Garini, Y., & Appelbaum, L. (2019). Sleep increases chromosome dynamics to enable reduction of accumulating DNA damage in single neurons. *Nature Communications*, *10*(1).

Zuleger, N., Robson, M. I., & Schirmer, E. C. (2011). The nuclear envelope as a chromatin organizer. *Nucleus*, *2*(5), 339–349.